NUCLEAR THEORY, Vol. 39 (2022)
eds. M. Gaidarov, N. Minkov, Heron Press, Sofia

Neutron Proton Asymmetry Effects in Far Fermi Energy Region

Sakshi Gautam, **Navjot K. Dhillon**, **Rajat Rana**

Department of Physics, Panjab University, 160014, Chandigarh

Abstract. Nuclear fragmentation of ^{124}Sn, ^{124}La + ^{nat}Sn collisions at 600 MeV/nucleon is studied using Isospin-dependent Quantum Molecular Dynamics (IQMD) model to investigate about the influence of isospin on the reaction dynamics. Charges of heaviest fragment and multiplicity of IMFs as a function of Z_{bound} are shown and these trends are not sensitive to N/Z of the system. However, a nice qualitative agreement with experimental measurement is noted. Further, nuclear stopping of intermediate mass fragments is studied. The degree of thermalisation of intermediate mass fragments is different due to different Coulomb interactions in both colliding pairs.

1 Introduction

On the basis of incident energy of projectile, heavy-ion collisions result in variety of phenomena ranging from fusion-fission at lower energies to complete disassembly of colliding matter at high beam energies. A reaction at intermediate energies produces several fragments of all sizes that may include free nucleons (FNs), light charged particles (LCPs), intermediate mass fragments (IMFs) and heavy mass fragments (HMFs). This phenomenon is known as multifragmentation [1, 2]. The first experiment to study the phenomenon of multifragmentation was performed using cosmic rays. Various statistical [3–5] and dynamical models [6–8] are developed to study the phenomenon of nuclear multifragmentation. In the statistical models reaction dynamics is negelected and it gives better description of final stage of reaction dynamics, whereas, in the dynamical models, the whole reaction dynamics from initial stage to final stage can be studied. In such models isospin effect comes via interplay of various reaction mechanisms such as Coulomb interaction, symmetry potential, mean field or nucleon-nucleon (*nn*) scattering cross-section, all of which are inputs to any theoretical approach. To get further insight about relative importance of these competing mechanisms, isobaric/isotopic colliding pairs are preferred. For charged particles, the Coulomb potential plays an important role and it sometimes competes strongly with the symmetry potential. One has to carefully disentangle effects of symmetry potential from those due to Coulomb potential. This symmetry potential has a strong density dependence and its sub-saturation behaviour is constrained (fairly well) with the help of various phenomena. On the contrary, the

density dependence of symmetry potential at supra-saturation densities is still a mystery, as different transport models present varied dependence. The nature of nuclear EOS of asymmetric nuclear matter will be resloved if this mystery is sorted out.

A systematic study of isospin effects in the breakup of projectile spectators at high energies has been performed with the ALADiN spectrometer at the GSI laboratory. The beams of ^{197}Au, ^{124}La, ^{124}Sn, ^{107}Sn are bombarded with ^{124}La, ^{124}Sn, ^{107}Sn target at 600 MeV/nucleon [9,10]. In this experiment it is observed that isotopic effects are small for global observables but most prominent feature of multifragment decay, i.e. universal rise and fall of fragment production when studied as a function of Z_{bound} ($Z_{\text{bound}} = \sum Z_{\text{frag}}$ with $Z_{\text{frag}} \geq 2$) is recovered. In this work, we aimed to study the role of isospin on the reaction dynamics of system having different N/Z ratio at high energies. The ^{124}La + ^{nat}Sn and ^{124}Sn + $^{\text{nat}}$Sn reactions have different isotopic ratio (N/Z) but same mass, and thus the bulk effects will be reduced and the difference in the outcome of such reactions will be governed by isospin effects. Therefore, these reaction pairs will be helpful in complete understanding of relative role of isospin effects at high energies. Here we have used the Isopin-dependent Quantum Molecular Dynamics (IQMD) model to study the multifragmentation of ^{124}Sn, ^{124}La + ^{nat}Sn at 600 MeV/nucleon.

2 Model

The IQMD model is an extension of the QMD model [6], which treats different charge states of nucleons, deltas and pions explicitly, as inherited from the Vlasov-Uehling-Uhlenbeck (VUU) model and which works on event-by-event basis. The isospin degree of freedom enters into the calculations via symmetry potential, *nn* scattering cross sections (and Pauli blocking) and Coulomb interactions.

In this model, baryons are represented by Gaussian-shaped density distributions

$$f_i(\vec{r},\vec{p},t) = \frac{1}{\pi^3\hbar^3}\exp\Big(-[\vec{r}-\vec{r_i}(t)]^2\frac{1}{2L}\Big)\exp\Big(-[\vec{p}-\vec{p_i}(t)]^2\frac{2L}{\hbar^2}\Big). \quad (1)$$

Nucleons are initialized in a sphere with radius $R = 1.12A^{1/3}$ fm, in accordance with the liquid-drop model. Each nucleon occupies a volume of h^3, so that phase space is uniformly filled. The initial momenta are randomly chosen between 0 and Fermi momentum ($\vec{p}_F$). The nucleons of the target and projectile interact by two-and three-body Skyrme forces, Yukawa potential, Coulomb interactions and symmetry potential. The hadrons propagate using the Hamilton equations of motion:

$$\frac{d\vec{r_i}}{dt} = \frac{d\langle H\rangle}{d\vec{p_i}}\,; \qquad \frac{d\vec{p_i}}{dt} = -\frac{d\langle H\rangle}{d\vec{r_i}} \quad (2)$$

with

$$\begin{aligned}\langle H\rangle &= \langle T\rangle + \langle V\rangle \\ &= \sum_i \frac{p_i^2}{2m_i} + \sum_i \sum_{j>i} \int f_i(\vec{r},\vec{p},t) V^{ij}(\vec{r}',\vec{r}) f_j(\vec{r}',\vec{p}',t) d\vec{r} d\vec{r}' d\vec{p} d\vec{p}'. \quad (3)\end{aligned}$$

The baryon potential V^{ij}, in the above relation, reads as

$$\begin{aligned}V^{ij}(\vec{r}'\vec{r}) &= V^{ij}_{Sky} + V^{ij}_{\text{Yuk}} + V^{ij}_{\text{Coul}} + V^{ij}_{\text{sym}} \\ &= [t_1\delta(\vec{r}'-\vec{r}) + t_2\delta(\vec{r}'-\vec{r})\rho^{\gamma-1}(\frac{\vec{r}'+\vec{r}}{2})] \\ &+ t_3 \frac{\exp(-|(\vec{r}'-\vec{r})|/\mu)}{(|(\vec{r}'-\vec{r})|/\mu)} + \frac{Z_i Z_j e^2}{|(\vec{r}'-\vec{r})|} + t_6 \frac{1}{\varrho_0} T_{3i} T_{3j} \delta(\vec{r_i}' - \vec{r_j}).\end{aligned}$$

Here Z_i and Z_j denote the charges of the i-th and j-th baryon, and T_{3i} and T_{3j} are their respective T_3 components (i.e. $1/2$ for protons and $-1/2$ for neutrons). The parameters t_1 and t_2 are related to nature of nuclear equation of state (EOS) of symmetric nuclear matter whereas $\mu = 0.4$ fm and t_3 correspond to range and strength of Yukawa potential and t_6 is related to the strength of symmetry potential. For the density dependence of nucleon potential, standard Skyrme-type parametrization is employed. We also use a standard energy-dependent free *nn* cross-section reduced by 20%, i.e. $\sigma = 0.8\sigma^{\text{free}}_{nn}$ [11]. The details about the elastic and inelastic cross sections for proton-proton and proton-neutron collisions can be found in Ref. [8]. The cross sections for neutron-neutron collisions are assumed to be equal to the proton-proton cross-sections. Two particles collide if their minimum distance d fulfills

$$d \leq d_0 = \sqrt{\frac{\sigma_{\text{tot}}}{\pi}}, \qquad \sigma_{\text{tot}} = \sigma(\sqrt{s}, \text{type}), \quad (4)$$

where 'type' denotes the ingoing collision partners ($N - N$ ...). Explicit Pauli blocking is also included, i.e. Pauli blocking of neutrons and protons is treated separately. We assume that each nucleon occupies a sphere in coordinate and momentum space. This trick yields the same Pauli blocking ratio as an exact calculation of the overlap of the Gaussians will yield. We calculate the fractions P_1 and P_2 of final phase space for each of the two scattering partners that are already occupied by other nucleons with the same isospin as that of scattered ones. The collision is blocked with the probability

$$P_{\text{block}} = 1 - [1 - \min(P_1, 1)][1 - \min(P_2, 1)], \quad (5)$$

and, correspondingly is allowed with the probability $1 - P_{\text{block}}$. Whenever an attempted collision is blocked, the scattering partners maintain the original momenta prior to scattering. The IQMD model generates phase space of nucleons and clusterization of these nucleons is required next to identify the fragments. The clusterization algorithm used here is minimum spanning tree (MST)

method [6]. The MST approach identifies fragments on the basis of spatial correlations among nucleons. In MST method, two nucleons will share the same cluster if distance between their centroids in coordinate space is less than $r_{\rm clus}$, i.e.,

$$|\vec{r_i} - \vec{r_j}| \leq r_{\rm clus}\,. \tag{6}$$

Here $\vec{r_i}$ and $\vec{r_j}$ are the centroids of the nucleons in coordinate space. Note that the value of $r_{\rm clus}$ may range from 2 fm – 5 fm. Here we have chosen $r_{\rm clus}$ to be 4 fm and it is worth noting that the value of $r_{\rm clus}$ does not alter the reaction outcome at final stage [12, 13]. There are various additions in MST method such as MST-B and MST-P which uses binding energy and momentum cut to identify the final fragments. It was already reported in one of our earlier studies [14] that the reaction outcome at final stage is independent of nature of the clusterization algorithm and thus conventional MST approach can be used to construct fragments.

3 Results and Discussion

Firstly, we have simulated the reactions of ^{124}Sn, ^{124}La + $^{\rm nat}$Sn at 600 MeV/nucleon over whole range of impact parameter from central to peripheral collisons. In Figure 1, we have shown the mean maximum charge ($Z_{\rm max}$, average charge of the heaviest fragment) normalized to the projectile charge ($Z_{\rm proj}$) as a function of the normalized bound charge $Z_{\rm bound}/Z_{\rm proj}$ for the collisions of: (a) ^{124}Sn + $^{\rm nat}$Sn;

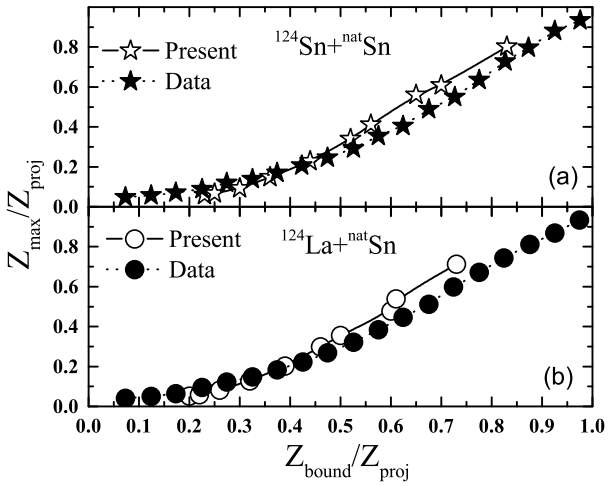

Figure 1. The mean maximum charge ($Z_{\rm max}$), normalized to the projectile charge ($Z_{\rm proj}$) as a function of the normalized bound charge $Z_{\rm bound}/Z_{\rm proj}$ for the collisons of: (a) ^{124}Sn + $^{\rm nat}$Sn; and (b) ^{124}La + $^{\rm nat}$Sn at 600 MeV/ nucleon. Calculated results (data) are represented by open (closed) symbols. Lines are only to guide the eye.

and (b) ^{124}La + ^{nat}Sn at 600 MeV/nucleon. Solid symbols show the experimental measurements [15] and open symbols display our calculations. With increasing $Z_{\rm bound}/Z_{\rm proj}$, the charge of heaviest fragments increases. This increase is gradual at lower $Z_{\rm bound}$ values and rises sharply for higher $Z_{\rm bound}$. Smaller $Z_{\rm bound}$ represents the central collisions where copious production of light charged particles take place, leading to lighter fragments. On the contrary, at semi-peripheral and peripheral collisions, the behaviour of $Z_{\rm max}/Z_{\rm proj}$ vs. $Z_{\rm bound}/Z_{\rm proj}$ is concave upwards which indicates that there is a reduced $Z_{\rm max}$ production with respect to a particular $Z_{\rm bound}$. This reduction governs the onset of multifragmentation where fragments produced are of intermediate mass range. The measured trends are qualitatively explained by our calculations. In order to investigate how the isotopic composition of the colliding partners affects the gross properties of the fragmentation pattern, multiplicity of IMFs ($3 \leq Z_f \leq 20$) is analyzed next. Figure 2 shows the multiplicity of IMFs as a function of $Z_{\rm bound}$ for the reactions of ^{124}Sn + ^{nat}Sn (top panel), ^{124}La + ^{nat}Sn (bottom panel). Experimental measurements are represented by symbols. Our calculations are represented by shaded bands and this shading corresponds to window of variation induced by two choices of IMFs viz. ($5 \leq A_f \leq 43$) and ($6 \leq A_f \leq 43$) [16] and inclusion and exclusion of ^{3}He in $Z_{\rm bound}$ definition. Note that the inclusion ^{3}He in the

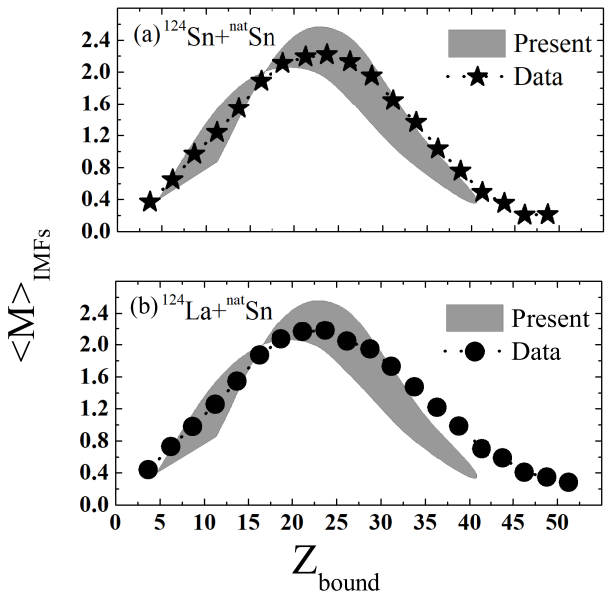

Figure 2. The multiplicity of IMFs as a function of $Z_{\rm bound}$ for the reactions of: (a) ^{124}Sn + ^{nat}Sn (top panel); and (b) ^{124}La + ^{nat}Sn (bottom panel). Shading in the figure corresponds to the two different ranges of IMFs viz., ($5 \leq A_f \leq 43$) and ($6 \leq A_f \leq 43$) and symbols are experimental measurements.

definition of Z_{bound} is done in the light of a study reported by Ref. [15] where significant production of ^{3}He can be observed at such energies during projectile fragmentation. Our calculations reasonably reproduce the measured trends in the yields of IMFs. It is also seen that reactions ^{124}La, ^{124}Sn + $^{\text{nat}}$Sn behave almost similarly. Thus, multiplicity of IMFs shows least sensitivity to extricate the isospin effects.

Further, we have investigated the stopping power of intermediate mass fragments (IMFs). There are various observables such as R_p, *vartl* and Q_{zz} which are used to study the degree of thermalisation acheived in a heavy-ion collisions. R_p is defined as [17, 18]

$$R_p = 2\sum_{i}^{M_f} p_t \Big/ \pi \sum_{i}^{M_f} p_z \,, \tag{7}$$

where p_t (p_z) are the transverse (longitudinal) momenta and $\sum$ is over all nucleons or fragments, where $p_t = \sqrt{p_x^2 + p_y^2}$.

vartl is the ratio of variances of the transverse to that of longitudinal rapidity distribution and is defined in Ref. [19, 20].

$$vartl = \frac{\langle y_x^2 \rangle}{\langle y_z^2 \rangle} \,, \tag{8}$$

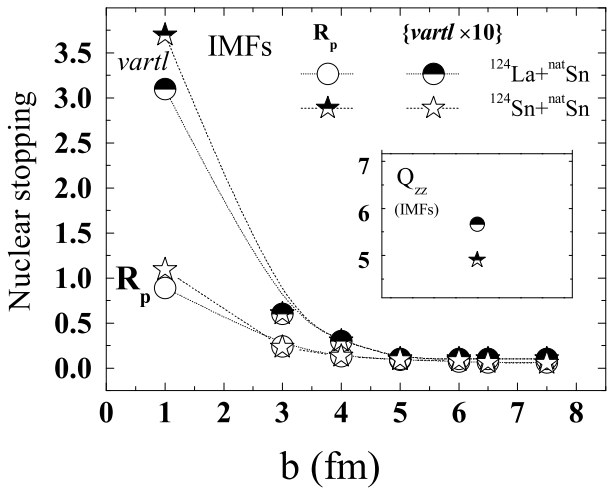

Figure 3. R_p and *vartl* (scaled by 10) of intermediate mass fragments (IMFs) for the reactions of ^{124}Sn + $^{\text{nat}}$Sn and ^{124}La + $^{\text{nat}}$Sn at 600 MeV/nucleon. Q_{zz} values for IMFs in central collisions ($b = 0-2$ fm) is shown in the inset. Lines are only to guide the eye.

where $\langle y_x^2 \rangle$ and $\langle y_z^2 \rangle$ are the variances of rapidity distribution of particles in the x and z directions. Quadrupole momentum is defined as [21];

$$\langle Q_{zz} \rangle = \sum_{i}^{M_f} [2p_z^2(i) - p_x^2(i) - p_y^2(i)] \,. \tag{9}$$

Figure 3, displays the nuclear stopping of IMFs as a function of impact parameter for the ^{124}Sn + ^{nat}Sn and ^{124}La + ^{nat}Sn collisions. In the inset are shown Q_{zz} for the central collisions ($b = 0-2$ fm). The *vartl* values are scaled by a factor of 10 for clarity. The stopping reduces as we move from central to peripheral collisions due to reduced nucleon nucleon collisions at peripheral geometries. Different thermalisation is achieved for IMFs in case of ^{124}Sn + ^{nat}Sn and ^{124}La + ^{nat}Sn reactions at central collisions. This behaviour is reflected in all stopping variables viz. R_p, *vartl* and Q_{zz} with IMFs produced in ^{124}Sn + ^{nat}Sn reaction showing better stopping compared to those produced in ^{124}La + ^{nat}Sn collisions.

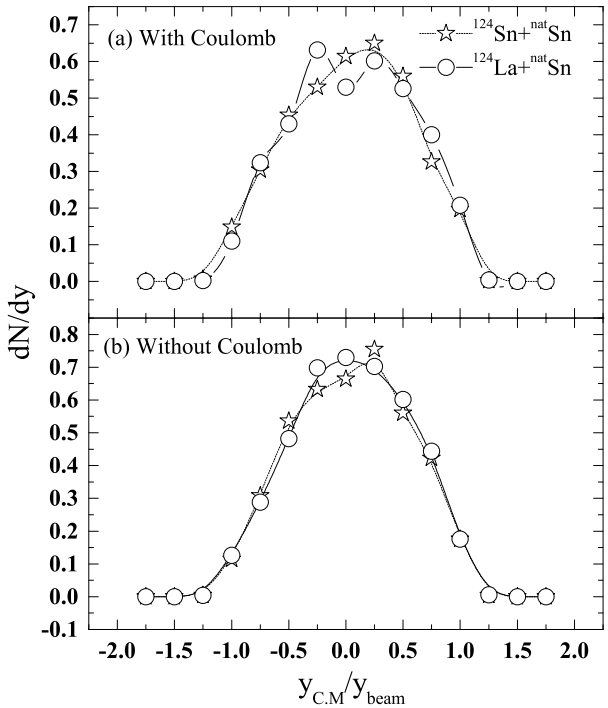

Figure 4. Rapidity distribution (dN/dy) of intermediate mass fragments (IMFs) in central collisions ($b = 0-2$ fm) of ^{124}Sn + ^{nat}Sn and ^{124}La + ^{nat}Sn at 600 MeV/nucleon. Top (Bottom) panel displays the results obtained with (without) Coulomb potential in the calculations. Lines are only to guide the eye.

In Figure 4, rapidity distribution (dN/dy) of IMFs are displayed for the calculations performed with and without Coulomb interactions. It has been observed that ^{124}La + ^{nat}Sn reaction has slightly wider distribution compared to ^{124}Sn + ^{nat}Sn reaction. But when calculations are performed without Coulomb interactions then this rapidity distribution gets narrow down. This is due to repulsive nature of Coulomb interactions which pushes the nucleons away from mid-rapidity. Thus a relatively weaker stopping of IMFs in ^{124}La + ^{nat}Sn collision is due to the fact that few IMFs are orginated from region away from mid-rapidity (because of repulsion induced by Coulomb interactions) and thus IMFs will have lower degree of thermalisation.

4 Conclusion

We have studied neutron proton asymmetry at energies away from Fermi energy. The nuclear stopping of IMFs is greater for the ^{124}Sn + ^{nat}Sn reactions incomparison to the ^{124}La + ^{nat}Sn reactions. This difference in thermalisation is due to different Coulomb interactions among this isobaric pair.

References

[1] B. Borderie, M.F. Rivet, *Prog. Part. Nucl. Phys.* **61** (2008) 551.

[2] J.P. Bondorf, A.S. Botvina, A.S. Iljinov, I.N. Mishustin, K. Sneppen, *Phys. Rep.* **257** (1995) 133.

[3] J.P. Bondorf, et al., *Nucl. Phys. A* **443** (1985) 321.

[4] A.S. Botvina, et al., *Z. Phys. A* **345** (1993) 297.

[5] S. Pal, S.K. Samaddar, J.N. De, *Nucl. Phys. A* **589** (1995) 489.

[6] J. Aichelin, *Phys. Rep.* **202** (1991) 233.

[7] R. . Puri, C. Hartnack, J. Aichelin, *Phys. Rev. C* **54** (1996) R28.

[8] C. Hartnack, et al., *Eur. Phys. J. A* **1** (1998) 151.

[9] W. Trautmann (ALADIN and INDRA collaborations), *Nucl. Phys. A* **787** (2007) 575.

[10] C. Sfienti et al., *Nucl. Phys. A* **749** (2005) 83c-92c.

[11] S. Gautam et al., *J. Phys. G: Nucl. Part. Phys.* **37** (2010) 085102.

[12] J. Singh, R.K. Puri, *Phys. Rev. C* **62** (2000) 054602.

[13] P.B. Gossiaux, D. Keane, S. Wang, J. Aichelin, *Phys. Rev. C* **51** (1995) 3357.

[14] R. Kumar, S. Gautam, R.K. Puri, *Phys. Rev. C* **89** (2014) 064608.

[15] C. Sfienti, et al., *Phys. Rev. Lett.* **102** (2009) 152701.

[16] A. Sharma, A. Bharti, S. Gautam, R.K. Puri, *Nucl. Phys. A* **945** (2016) 95.

[17] G. Lehaut, et al., *Phys. Rev. Lett.* **104** (2010) 232701.

[18] R.E. Renfordt, D. Schall, *Phys. Rev. Lett.* **53** (1984) 763.

[19] W. Reisdorf, et al., *Phys. Rev. Lett.* **92** (2004) 23.

[20] Y. Yuan, Q. Li, Z. Li, F.H. Liu, *Phys. Rev. C* **81** (2010) 034913.

[21] J.Y. Liu, et al., *Phys. Rev. Lett.* **86** (2001) 975.